RSC Advances

ROYAL SOCIETY OF CHEMISTRY

www.rsc.org/advances

Theoretical Study of Surface Dependence of NH_3 Adsorption and Decomposition on Spinel-type $MgAl_2O_4$

Huan Wang,[a] Chuanyi Jia,[b] Jing Yang,[a] Xian Zhao,[b] Yanlu Li,[b] Honggang Sun,[c] and Weiliu Fan*[a]

a) School of Chemistry and Chemical Engineering, Shandong University, Jinan 250100 China

b) State Key Laboratory of Crystal Materials, Shandong University, Jinan 250100 China

c) School of Environmental Science and Engineering, Shandong University, Jinan 250100 China

Electronic Supplementary Information (ESI) available: The convergence surface energies for the different layers of the three surfaces; all the possible configurations of NH_3 molecule adsorbing on different sites; the treatment of the surface polarity; the models of the oxygen vacancy; the configurations of NH_3 adsorbing on defective surfaces.

ABSTRACT

Ammonia decomposition is a critical process in the production of renewable hydrogen energy. Although many studies have concentrated on ammonia decomposition, little is known about the effect of the spinel support on the activation of NH_3. The adsorption and dissociation of NH_3 on low-index (100), (110), and (111) $MgAl_2O_4$ surfaces were investigated using density functional theory. The interaction between NH_3 and $MgAl_2O_4$ was structure dependent, with the surface geometry and electronic structures determining the active sites and adsorption stability. The NH_3 was likely to point toward a surface protruding metal site with the formation of a hydrogen bond. For dissociation, the adsorption energy of the (111) surface was much more favorable than the energies of the (100) and (110) surfaces. The surface Al_{3c}-sp state at the Fermi level and the formation of the H-O_{3c} covalent bond of this surface were the main reasons for the higher adsorption energy in NH_3 dissociation. In particular, the hybridization between the Al_{3c}-sp state and N-p state on the (111) surface was larger than those of the other two surfaces. In view of the thermodynamics and dynamics, the (111) surface was more favorable for NH_3 adsorption and reaction. For the defective surfaces, the existence of an oxygen vacancy lowered the adsorption ability

* To whom all correspondences should be addressed. Tel: 86-531-88366330, Fax: 86-531-88364864, E-mail: fwl@sdu.edu.cn

on metal sites. This was due to the destroyed surface symmetry structure and the reduced charge of the metal site. In addition, only on the (111) surface could the oxygen vacancy act as an active site for adsorption. The energy barrier of NH_3 dissociation on the Vo_{3c} (111) surface was the lowest, which indicated that the NH_3 reaction on this defective surface was dynamically the most favorable. These findings have an important implication for the decomposition of NH_3 on $MgAl_2O_4$ surfaces and could provide theoretical guidance for other catalytic reactions.

Keywords: NH_3, reaction, spinel $MgAl_2O_4$, density functional theory (DFT), structure dependent

1. INTRODUCTION

Ammonia has been used as the hydrogen source and storage material in fuel cells [1-6]. The catalytic decomposition of ammonia could produce a clean hydrogen fuel, which could be an effective way to solve the current energy problems, although ammonia (NH_3) is a toxic gas that could cause environmental pollution. Therefore, the catalytic dissociation of ammonia has important significance for solving energy and environmental problems. Composite catalysts have often been used for heterogeneous catalytic reactions. These materials have included transition metals (active components) and supports. Generally, the support of the catalyst has been a base material providing dispersion, support, and stability to the metal active phase. It has also been reported that the support played an essential role in the activation between the catalyst and adsorbate. For example, an alumina support could improve the reaction activity of a metal catalyst in the catalytic process [7-8]. However, some reports have indicated that the support could participate in the reaction without a metal phase: the alumina could directly activate the CO, CH_4 [9-10], and ethanol [11] molecules. These reports indicated that the catalysis was complex. They also suggested that it was necessary to systematically investigate the interaction in the heterogeneous catalytic reaction in order to understand the catalysis mechanism, optimize the catalytic system, and design a highly efficient catalyst.

The spinel $MgAl_2O_4$ material, which shows much more stability and mechanical strength than some other oxides, was an effective support for an ammonia reaction [12,

13]. Szmigiel et al. investigated ammonia decomposition over Ba- or Cs-doped Ru catalysts deposited on the $MgAl_2O_4$ support [13]. A multi-composite oxide possesses a complex surface structure in comparison with a single oxide, which would allow better properties. Thus, the microscopic surface structure of $MgAl_2O_4$ was controllable for the ammonia reaction. It is well known that the surface atom arrangements and active sites are different for different surfaces, which would likely result in different adsorption behaviors [14-18]. In addition, the establishment of oxygen vacancies would change the atomic and electronic surface structure, resulting in different adsorption behaviors [19]. The surface chemical properties of an oxygen defective surface would be different from those of a perfect surface [20-22]. Moreover, oxygen vacancies have been found to be important reactive sites on a surface [19, 23]. Besenbacher et al. demonstrated that the oxygen vacancies of a TiO_2 surface were active sites for water dissociation. Thus, it was necessary to pay attention to the ammonia reaction properties on oxygen defective $MgAl_2O_4$ surface.

In this work, we concentrated on the ammonia adsorption and decomposition on perfect and defective $MgAl_2O_4$ (100), (110), and (111) surfaces. The surface structure-activity relationship was complicated, and it was necessary to perform a detailed investigation. Three low-index stoichiometric $MgAl_2O_4$ surfaces were selected to explore its structural sensitivity and surface electronic structure. This paper is organized as follows. Section 2 describes the computational methods used. Section 3 presents and discusses the results of a theoretical analysis of NH_3 adsorption on perfect and defective $MgAl_2O_4$ surfaces. Section 4 summarizes the main conclusions.

2. COMPUTATIONAL METHODS AND SURFACE MODELS

The calculation of the NH_3 reaction with $MgAl_2O_4$ was performed with density functional theory (DFT) [24] calculations using CASTEP [25]. The core-electron interaction was described using ultrasoft pseudopotentials [26]. For Mg, the 2p and 3s states (8 electrons) were treated as valence states. For Al, the 3s and 3p states (3 electrons) were treated as valence states, and for O, the 3s and 3p states (6 electrons) were treated as valence states. After the NH_3 adsorption, for N, the 2s and 2p states (5 electrons) were treated as valence states, whereas for H, the 1s state (1 electron) was

treated as a valence state. The generalized gradient approximation (GGA) proposed by Perdew and Wang in 1991 (PW91) [27, 28] was employed for the exchange and correlation functional. The self-consistent convergence accuracy was set at 2.0×10^{-6} eV/atom, and the convergence criterion for the maximal force between atoms was 0.05 eV/Å. The maximum displacement was 0.002 Å, and the stress was 0.1 GPa. The wave functions were expanded in a plane wave basis set, while the specified cutoff energy was set at 340 eV, and this cutoff energy was used throughout the calculations. Monkhorst–Pack [29] grids of $3 \times 3 \times 3$ κ-points were used for the bulk unit cell, and grids of $2 \times 2 \times 1$ κ-points were used for the (100), (110), and (111) surfaces.

The bulk crystal structure of the spinel $MgAl_2O_4$ was calculated, along with the results of the lattice parameters ($a = b = c = 8.20552$ Å, $\alpha = \beta = \gamma = 90°$), which remained consistent with the experimental parameters ($a = b = c = 8.08060$ Å, $\alpha = \beta = \gamma = 90°$) [30]. The main exposed low-index surfaces of $MgAl_2O_4$ included the (100), (110), and (111) surfaces. A careful convergence test had to be conducted to choose the proper slab terminations and slab thickness. After this calculation, we found that the Mg-O-Al terminated surfaces had lower surface energies than the Mg-O or Al-O terminated surface (Table 1). Thus, the Mg-O-Al terminated surfaces were considered to be the adsorption surfaces. In order to choose the proper number of slab layers, detailed convergence tests were conducted. The following surfaces were used for the test slab thickness (Table S1, ESI): (100) for 5, 7, and 9 slab layers; (110) for 5, 6, and 7 slab layers; and (111) for 5, 7, and 9 slab layers. The three surfaces converged to 0.02 eV/Å^2, 0.01 eV/Å^2, and 0.01 eV/Å^2 respectively, which were within 0.065 eV/Å^2 of each other [31]. Therefore, to keep the computational cost low, we only chose seven layers for the (100) and (111) surfaces and six layers for the (110) surface as the calculation models to study ammonia adsorption in the present work. Thus, the $MgAl_2O_4$ (100) surface was modeled using a periodic 2×2 surface unit cell, with 16 units possessing 112 atoms. The (110) surface was modeled using a periodic 2×1 surface unit cell, with 12 units possessing 84 atoms, and the (111) surface was modeled using a periodic 2×2 surface unit cell, with 16 units possessing 112 atoms. To separate the layer and its images in the direction perpendicular to the magnesium

aluminate plane, we chose 20 Å as the vacuum region. Before the geometry optimization of the three surfaces, the top three layers were selected to relax, while the remaining layers were constrained to model the bulk effects. Moreover, because the three surfaces are polar, particular treatments [32-35] are employed to eliminate the polarity of the surface in Figure S4 (ESI). The results of NH_3 adsorption and reaction on $MgAl_2O_4$ indicated that the polarity played little effect on the selectivity of surface active sites and the NH_3 dissociation process (Figures S5-S7, ESI). A Mulliken population analysis [36, 37] was performed to determine the charge transfers and population to gain an understanding of the nature of bonding and the interaction between the NH_3 and $MgAl_2O_4$ surfaces.

The adsorption energy E_{ads} was used to evaluate the interaction of the NH_3 with the magnesium aluminate spinel, and it was calculated as follows:

$$E_{ads} = \left[E_{slab} + E_{NH_3} \right] - E_{slab/NH_3}$$

where E_{slab} and E_{NH_3} are the total energies of the pristine $MgAl_2O_4$ and free NH_3 molecule, respectively, and E_{slab/NH_3} is the total energy of the slab with the adsorbed or dissociative-adsorbed NH_3 molecule. On the basis of the above definitions, negative values of adsorption energy corresponded to an endothermic process, whereas positive values indicated that the adsorption was thermodynamically favorable. In order to accurately determine the activation barriers of the reaction, we chose the complete linear and quadratic synchronous transition (LST/QST) approach to search for the transition states (TS) of the reactions [38]. The complete LST/QST approach combines the LST algorithms for constrained minimizations with the QST algorithm. An LST/optimization calculation is first performed. Then, the QST maximization is performed to obtain the TS approximation. After this, another constrained minimization is performed, and the cycle is repeated until a stationary point is found, or the number of allowed steps is exhausted. In this system, a value of 0.25 eV was employed for the RMS convergence, while the maximum number of QST steps was five.

Table 1. Surface energies of (100), (110), and (111) surfaces with different terminations

Surface plane	Termination	Surface energy (J/m^2)
(100)	Al-Mg-O	1.37
	Al-O	2.98
(110)	Al-Mg-O	1.81
	Al-O	3.26
(111)	Al-Mg-O	2.00
	Mg-O	4.58

3. RESULTS AND DISCUSSION

3.1 NH_3 Adsorption and Dissociation on Perfect $MgAl_2O_4$ Surfaces

3.1.1 Structure of Perfect $MgAl_2O_4$ Surfaces

We first investigated the optimized perfect structures of $MgAl_2O_4$ (100), (110), and (111) surfaces, as seen in Figure 1. It was easy to find that the three surfaces all consisted of unsaturated metal (Mg and Al) and oxygen atoms, but differed in their degree of unsaturation and surface atom arrangement. The unsaturated atoms located at the outermost surfaces were separately labeled as 2-fold-coordinated Mg (Mg_{2c}), 3-fold-coordinated Mg (Mg_{3c}), 3-fold-coordinated Al (Al_{3c}), 4-fold-coordinated Al (Al_{4c}), 5-fold-coordinated Al (Al_{5c}), 3-fold-coordinated O (O_{3c}), and 4-fold-coordinated O (O_{4c}). For the (100) surface, Mg_{2c} protruded from the plane and Al_{5c} was surrounded by four oxygen atoms, which acted as metal adsorption sites. O_{3c} was a favorable site for bonding the H atom, which acted as an O adsorption site. For the (110) surface, the metal adsorption sites included Mg_{3c} and Al_{4c}. The difference compared with the (100) surface was that the two types of metal atoms were both located under the surface. The O_{3c} site slightly protruded from the surface to capture the H atom. The (111) surface possessed a different structure compared with the other two surfaces. The Al_{3c} atoms protruded from the surface, while the O_{3c} atom was isolated in the center. In Table 2 are listed the vertical displacements of the surface

atoms relative to their bulk positions that have been calculated from the equilibrium slab geometry. For the $MgAl_2O_4$ (100) surface, the Mg atom considerably relax outward by 0.023 Å, the Al atom move inward by 0.062 Å, the O_{3c} and O_{4c} atoms move outward by 0.057 Å and 0.277 Å. For the (110) and (111) surfaces, the metal and O_{3c} atoms move inward by 0.001-0.463 Å, the O_{4c} atoms move outward by 0.121-0.171 Å. This indicates that the $MgAl_2O_4$ surface remains stable in the full-geometry optimization, the presence of unsaturated atoms do not distort the surface upon relaxation.

Table 2. Comparison of the vertical relaxation of the top surface atoms for the bare (100), (110) and (111) surfaces of $MgAl_2O_4$.

Surface	z-shifts/Å			
	Mg	Al	O_{3c}	O_{4c}
(100)	0.023	-0.062	0.057	0.277
(110)	-0.043	-0.463	-0.029	0.171
(111)	-0.088	-0.109	-0.001	0.121

To further examine the effect of the surface electronic structure on the NH_3 adsorption reaction, we calculated the Mulliken charge (as seen in the top view of Figure 1). Although the absolute value of this charge was meaningless, the difference between the charge values before and after NH_3 adsorption showed us the charge transfer, which determined the adsorption behavior. Our calculation demonstrated that the surface metal atoms carried a positive charge, while the surface oxygen atoms carried a negative charge. The different charge values of the surface metal and oxygen atoms determined the bonding properties between the NH_3 and surface atoms.

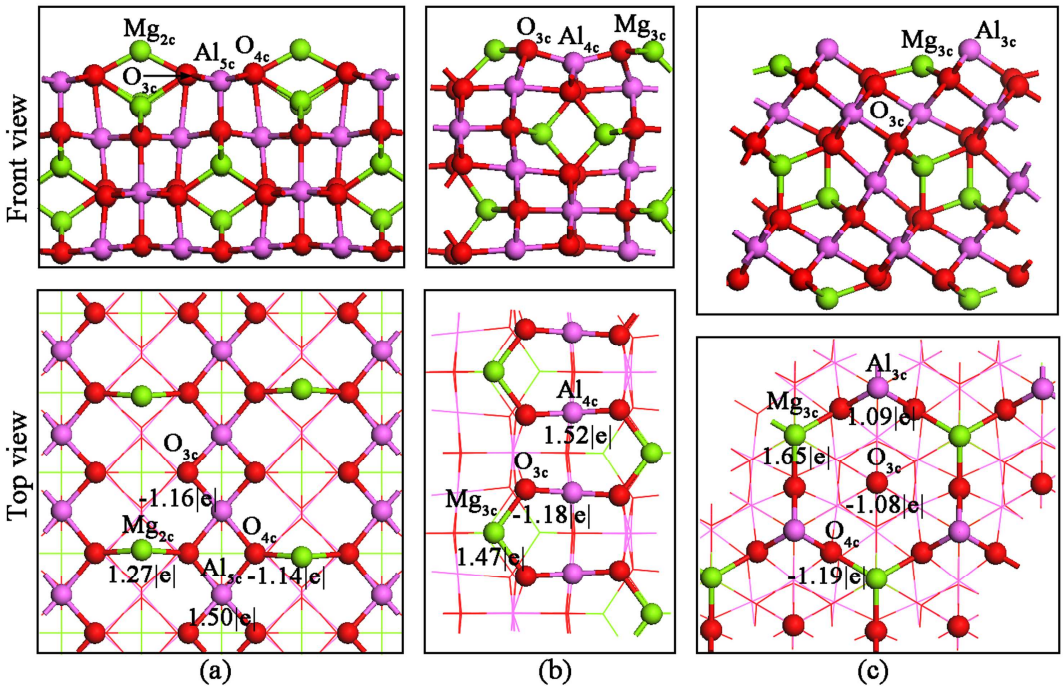

Figure 1. Front and top views of optimized surface structures: **(a)** (100) surface, **(b)** (110) surface, and **(c)** (111) surface. The surface sites and Mulliken charges carried by these are labeled in the top view of each surface. Color coding: red, O atoms; purple, Al atoms; green, Mg atoms.

The surface geometric and electronic structures would coordinately influence the adsorption and reaction, which would lead to a complex surface adsorption. Therefore, to correlate the surface atomic and electronic structures with the catalytic activity, the interactions between the NH_3 molecule and surfaces of the $MgAl_2O_4$ catalyst were carefully examined and are thoroughly discussed in the following sections.

3.1.2 Interaction of NH_3 with Perfect Surfaces

The NH_3 molecule could interact with the $MgAl_2O_4$ (100), (110), and (111) perfect surfaces in several different ways by utilizing H atoms and protruding N atoms. This section will discuss the molecular and dissociated adsorption conditions of the three surfaces. Five models were constructed to determine the adsorption energy of the $MgAl_2O_4$ system (Figure 2). Figure 2a is a model that the NH_3 molecule adsorbs via one H atom to the surface. Figure 2b has a bridging configuration with two H atoms of NH_3 binding with two O atoms. Figure 2c shows a single N-adsorbed model adsorbed via a surface metal atom. Figure 2d shows a model of the participation of the

N-M bond and hydrogen bond, which generates a bidentate bonding species. In Figure 2e, the N atom pointes toward the metal atom, while bridged hydrogen bonds are formed. Based on the five models, all of the possible adsorption models of the NH_3 molecule with various orientations and different adsorption sites were calculated and are presented in Figures S1-S3 (ESI).

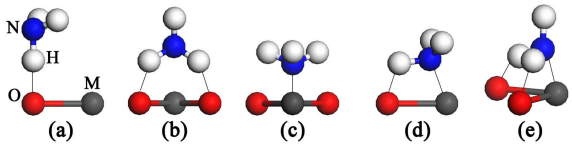

Figure 2 Possible models of NH_3 adsorbed on $MgAl_2O_4$ surfaces. Color coding: gray, M atoms (M = metal); red, O atoms; blue, N atoms; white, H atoms.

***(100) Surface**:* Several types of the most favorable configurations for the NH_3 adsorption and reaction on the (100) surface are presented in Figure 3. When we calculated the adsorption model that the NH_3 molecule adsorbs via one H atom to the surface, the N atom would shift to form the N-Mg_{2c} bond [Figure S1, ESI]. This proved that the metal atom was the main active site for adsorption. The metal active sites included the Al_{5c} and Mg_{2c} atoms. The strong steric hindrance prohibited the adsorption on the Al_{5c} site, for which the adsorption energy was only 0.61 eV (Figure 3a). It was easy to find that the adsorption on the Mg_{2c} site was more favorable than that of the Al_{5c} site. This was because the Mg_{2c} atom protruded from the surface without hindrance. As seen in Figure 3b and Figure 3c, the adsorption energy increases by 0.09 eV with the participation of the H-O_{3c} bond on the Mg_{2c} site. This suggests that the hydrogen bond had a synergic effect on the adsorption. The dissociated structure is presented in Figure 3d. When the surface Mg_{2c} pointed to the N atom, and O_{3c} bonded with the dissociated H atom to form the H-O_{3c} bond, this bond, with a length of 0.99 Å, was a covalent bond, which would have promoted the dissociation. However, the adsorption energy was only 1.03 eV, which was much lower than the favorable molecular adsorption energy (1.64 eV). Moreover, the adsorption energy of the NH_3 dissociated adsorption was much lower than that (1.55

eV) of the molecular adsorption without the hydrogen bond. Thus, the difference could not be explained using only the geometric structure. Therefore, the Mulliken charges presented in Table 3 were employed to analyze the surface electronic structure and explain the distinct adsorption energies. There was little difference in the charge values before and after the adsorption on the Al site, which resulted in the lowest adsorption energy on the Al_{5c} site. The change in the charge on the Mg_{2c} site was complex. A large number of charges increased (0.35 |e| and 0.36 |e|) on the Mg_{2c} site for molecular adsorption, and the charge increased by 0.24 |e| on the Mg_{2c} site for dissociation. This indicated that the strong interaction between the NH_3 and Mg_{2c} during the NH_3 molecular adsorption and reaction. However, the change in the charge on NH_3 was very different. For adsorption without the hydrogen bond, the NH_3 charge changed by 0.05 |e|. The charge decreased by 0.11 |e| for the molecular adsorption with the hydrogen bond. The NH_3 could obtain an electron from the surface oxygen through the hydrogen bond. For the dissociation, the NH_3 charge decreased by 0.36 |e| (Table 3d), which was a larger decrease than that of the molecular adsorption. This was because the NH_2 group obtained an electron from the dissociated H atom. Meanwhile, this H atom obtained an extra electron from the surface O_{3c} site. The effect of the left electron state on the N atom would play another role in the NH_3 dissociation.

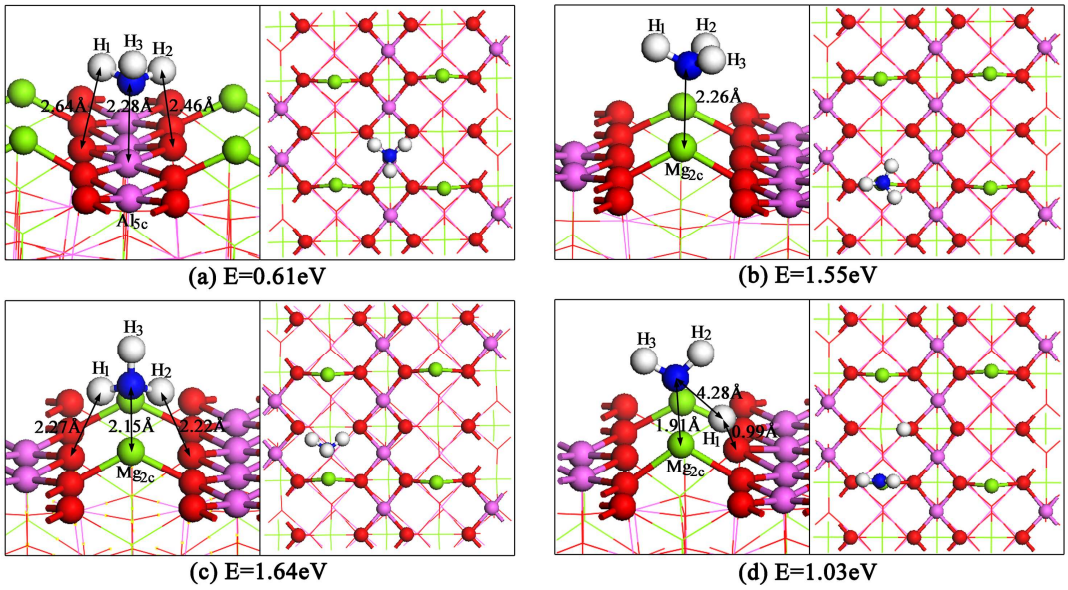

Figure 3. Front and top views of the most favorable adsorption configurations and energies of NH_3 on a perfect (100) surface: **(a)** NH_3 pointing towards the Al_{5c} atom, **(b)** NH_3 perpendicular to the surface Mg_{2c} atom, **(c)** two H atoms pointing towards O_{3c} atoms on the Mg_{2c} site, and **(d)** dissociation on the Mg_{2c} site.

Table 3. Mulliken charges for clean and adsorbed (100) surface, where **clean** corresponds to perfect surface configuration without NH_3 adsorption and **(a–d)** correspond to configurations in Figure 3.

Mulliken charges, |e|		N	H_1	H_2	H_3	NH_3	Mg	Al	O_{3c1}	O_{3c2}
(100)	Clean	-1.26	0.42	0.42	0.42	0	1.27	1.50	-1.16	-1.16
	(a)	-1.10	0.36	0.37	0.37	0	1.27	1.51	-1.17	-1.17
	(b)	-1.23	0.40	0.39	0.39	-0.05	1.62	1.49	-1.16	-1.16
	(c)	-1.18	0.34	0.34	0.39	-0.11	1.63	1.48	-1.16	-1.16
	(d)	-1.38	0.39	0.32	0.31	-0.36	1.51	1.53	-1.01	-1.17

To further analyze the surface electronic properties, the local density of states (LDOS) was calculated in this work (Figure 4). A comparison of Figure 4a and Figure 4b shows an obvious peak (Mg_{2c}-s state) at the Fermi level in Figure 4b, with the special Mg_{2c}-s state disappearing after the NH_3 adsorption and reaction. The Mg_{2c}-s

state was called the surface state. Normally, the surface state originated from the dangling bonds at the surface, which could affect the electron density distribution of the surface. This suggested that the existence of the surface state had an effect on the chemical reaction [39-40]. The energy obtained from the disappearing surface Mg_{2c}-s state drove the NH_3 adsorption, which indicated that the surface state contributed to the favorable adsorption on the Mg_{2c} site. The LDOS of the surface O_{3c} atoms was further analyzed. For the molecular adsorption, the O_{3c}-p state showed little change. For the dissociated adsorption, the bonding interaction between the dissociated H atom and the surface O_{3c} atom was very strong, which resulted in an obvious downshift in the O_{3c}-p state. Thus, the system energy decreased. It was easy to find that the H-O_{3c} bond was a covalent bond, which was an important force for the dissociation. In Figure 4c, the Mg_{2c}-s orbital overlaps with the N-sp orbital at the valence band, which verifies the bonding between the NH_3 and surface Mg_{2c} atom. In addition, the N-sp peaks was different between the molecular adsorption and dissociated adsorption. For the dissociation, a new N-sp state at the -1.05-eV position appeared near the Fermi level, which originated from the left electron state of the dissociated H atom. This corresponded to the 0.12 |e| reduction in the charge value of the N atom (Table 3d). The N-sp state was located between -9.50 eV and -6.05 eV for the molecular adsorption, whereas the new state obviously drove the N-sp state shift toward a higher energy (between -6.43 eV and -3.74 eV) for the dissociated adsorption. The up-shift of the N-sp state of dissociation gave the system greater disability compared with the system of molecular adsorption. The new N-sp state caused a large electron gathering at the N atom, which resulted into the disability of the NH_3 dissociation on the Mg_{2c} site. Therefore, from the viewpoint of thermodynamics, the molecular adsorption on the Mg_{2c} site of the (100) surface was more favorable than that of the dissociation.

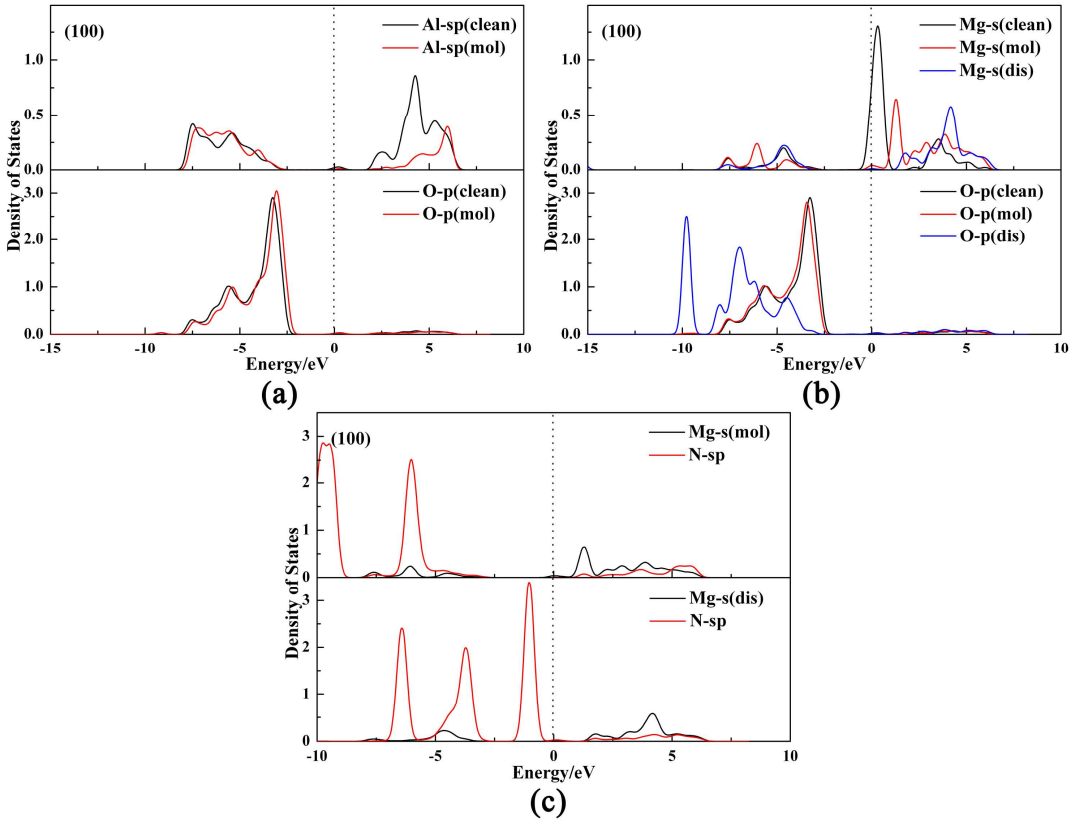

Figure 4. LDOS of (100) surface: **(a)** clean surface and molecular adsorption on Al_{5c} site, **(b)** clean surface and adsorption on Mg_{2c} site, and **(c)** comparison between molecular and dissociated adsorptions on Mg_{2c} site. The Fermi level is shown by the vertical dotted line.

(110) Surface: The surface structures and corresponding adsorption energies of NH_3 on the perfect (110) surface are given in Figure 5. The (110) surface has the similarity of the active centers and its distributions with (100) surface, thus the adsorption models of (110) surface are similar to that of (100) surface. Mg_{3c} and Al_{4c} were still the active sites for NH_3 adsorption. The adsorption on the Mg_{3c} site was more favorable than that on the Al_{4c} site, which suffered from strong steric hindrance. However, the adsorption energies on the metal sites for the (110) and (100) surfaces were rather distinct. The adsorption energy on the Mg_{3c} site decreased to 1.01 eV, because the Mg_{3c} atom was located under the (110) surface, which was a disadvantage for adsorption compared with the protruding Mg_{2c} atom of the (100) surface. For the adsorption on the Al_{4c} site, the adsorption energy increased to 0.88 eV, which could

be explained by the synergetic effect of two Al_{4c} atoms. In order to explore the influence of the hydrogen bond, we established a special model, as shown in Figure 5c, which possessed two hydrogen bonds without the participation of the Mg_{3c} site. The adsorption energy of this structure was relative low, which proved the minor effect of the hydrogen bond on adsorption. The dissociation occurred at the Al_{4c} site of the (110) surface, which was different from that of the (100) surface. The surface geometry structure twisted after the NH_3 dissociation on the Al_{4c} site, which resulted in the instability of the system. When we calculated the NH_3 dissociation on the Mg_{3c} site, we found that the H atom would reunite with the NH_2 group to form an NH_3 molecule because the surface O_{3c} atom remained close to the Mg_{3c} atom, which suggested that dissociation on the Mg_{3c} site of the (110) surface was impossible.

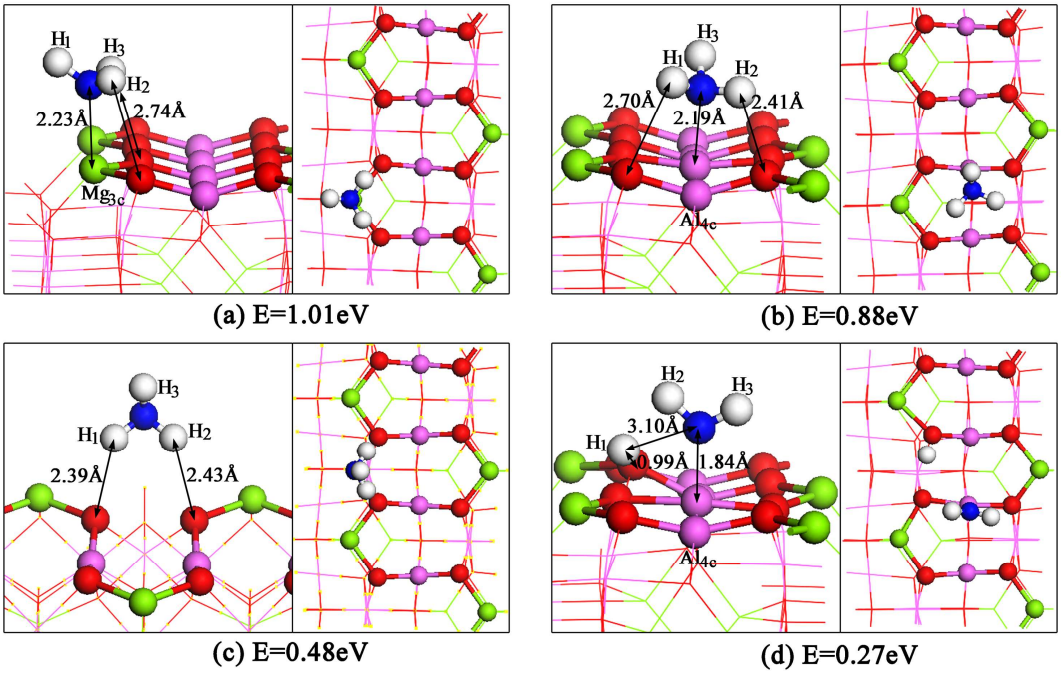

Figure 5. Front and top views of most favorable adsorption configurations and energies of NH_3 on perfect (110) surface: (**a**) NH_3 pointed toward Mg_{3c} atom, (**b**) NH_3 located between two Al_{4c} atoms, (**c**) two H atoms pointed toward O_{3c} atoms, and (**d**) dissociation on Al_{4c} site.

Table 4. Mulliken charges for clean and adsorbed (110) surface, where **clean** corresponds to

perfect surface configuration without NH_3 adsorption and **(a–d)** correspond to configurations in Figure 5.

Mulliken charges, |e|		N	H_1	H_2	H_3	NH_3	Mg	Al	O_1	O_2
	clean	-1.26	0.42	0.42	0.42	0	1.47	1.52	-1.18	-1.18
	(a)	-1.21	0.36	0.36	0.39	-0.10	1.72	1.52	-1.17	-1.18
(110)	(b)	-1.11	0.40	0.41	0.36	0.06	1.44	1.52	-1.16	-1.17
	(c)	-1.13	0.33	0.34	0.41	-0.05	1.49	1.52	-1.17	-1.18
	(d)	-1.25	0.41	0.35	0.35	-0.14	1.47	1.45	-1.06	-1.17

The Mulliken charges were calculated to analyze the electronic structure presented in Table 4. A much greater variation in the charge values before and after the molecular adsorption on the Mg_{3c} site (Table 4a) is seen, which proves that the Mg_{3c} atom is the main active site. The charge did not change on the Al_{4c} site for the molecular adsorption. For the dissociation, the charge decreased from 1.52 |e| to 1.45 |e| on the Al_{4c} site, which was different from the other metal sites (the charge increased after adsorption). The electron transferred to the Al_{4c} atom, which lowered the interaction between the NH_3 and Al_{4c} site. The variation in the charge on the NH_3 molecule of the (110) surface was related to the hydrogen bond and dissociated state, which were consistent with those of the (100) surface.

The LDOS was employed to further analyze the surface electronic structure, as seen in Figure 6. The surface Mg_{3c}-s state was easy to find, while no obvious Al_{4c}-sp state was found at the Fermi level. Therefore, the surface Mg_{3c}-s state contributed to the favorable adsorption stability on the Mg_{3c} site. As shown in Figure 6b, the Al_{4c}-sp did not shift during molecular adsorption, whereas the Al_{4c}-sp state at the valence band shifted to a higher energy band. This hindered the dissociated adsorption, which corresponded to a reduction in the charge value on the Al_{4c} atom. For the dissociation on the Al_{4c} site, the dissociated H combined with the surface O_{3c} to form the H-O_{3c} covalent bond. This investigation showed that the molecular adsorption on the Al_{4c} site was more stable than the dissociation on the Al_{4c} site. In summary, we concluded

that the molecular adsorption on the Mg_{3c} site was the most favorable thermodynamically on the (110) surface.

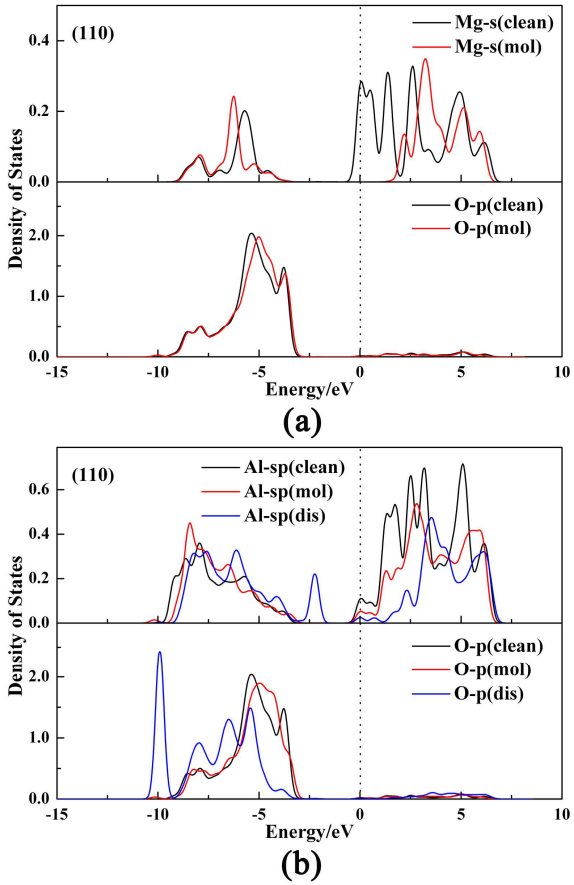

Figure 6. LDOS of (110) surface: **(a)** clean surface and molecular adsorption on Mg_{3c} site and **(b)** clean surface and adsorption on Al_{4c} site.

(111) Surface: Figure 7 presents the favorable adsorption configurations and energies. The NH_3 molecule was more inclined to be adsorbed at a position that combined the active metal sites (Al_{3c} and Mg_{3c} sites) and generated hydrogen bonds. Compared with the adsorption energies, the most favorable adsorption site was the Al_{3c} site, which was different from those for the former two surfaces. This was because the Al atom protruded from the surface. The Mg_{3c} was located under the Al_{3c} atoms, which suffered from steric hindrance and adsorption competition from the nearby Al_{3c}. As seen in Table 5, the changes in the Mulliken charges on the Al_{3c} and Mg_{3c} atoms could also illustrate the adsorption difference: the charge value increased

by 0.61 |e| on the Al_{3c} site, while it only increased by 0.14 |e| on the Mg_{3c} site. We calculated the dissociation on the Mg_{3c} site and found that the NH_2 would shift to the Al_{3c} atom. This meant that dissociated adsorption was inclined to occur on the Al_{3c} site. Figure 5c presents the dissociation configuration on the Al_{3c} site. Its adsorption energy was 3.07 eV, which was much higher than that of the molecular adsorption (2.02 eV). The difference in the charge transfer values on the Al_{3c} site for the molecular and dissociated adsorptions was quite small, and could not be used to explain this large adsorption energy difference. Therefore, the LDOS was employed to explain the different energies, as seen in Figure 8.

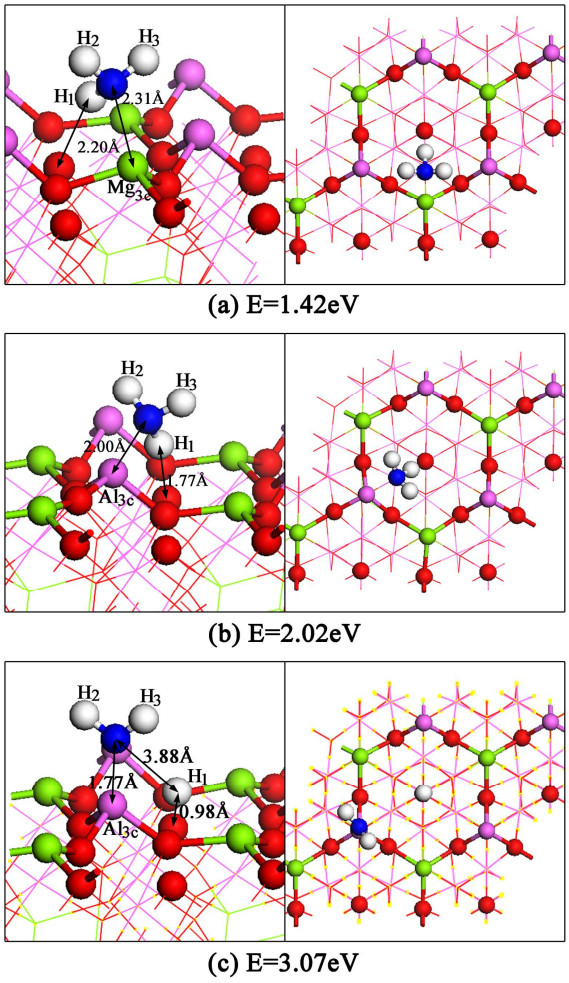

Figure 7. Front and top views of most favorable adsorption configurations and energies of NH_3 on perfect (111) surface: **(a)** H_1 pointed toward O_{3c} atom on Mg_{3c} site, **(b)** H_1 pointed toward O_{3c}

atom on Al_{3c} site, and **(c)** dissociation on Al_{3c} site.

Table 5. Mulliken charges for clean and adsorbed (111) surface, where c**lean** corresponds to perfect surface configuration without NH_3 adsorption and **(a–d)** correspond to configurations in Figure 7.

Mulliken charges, |e|		N	H_1	H_2	H_3	NH_3	Mg	Al	O_{3c}
(111)	clean	-1.26	0.42	0.42	0.42	0	1.65	1.09	-1.08
	(a)	-1.17	0.33	0.34	0.34	-0.16	1.79	1.03	-1.08
	(b)	-1.14	0.38	0.40	0.40	0.04	1.59	1.70	-1.07
	(c)	-1.35	0.41	0.39	0.37	-0.18	1.62	1.68	-0.96

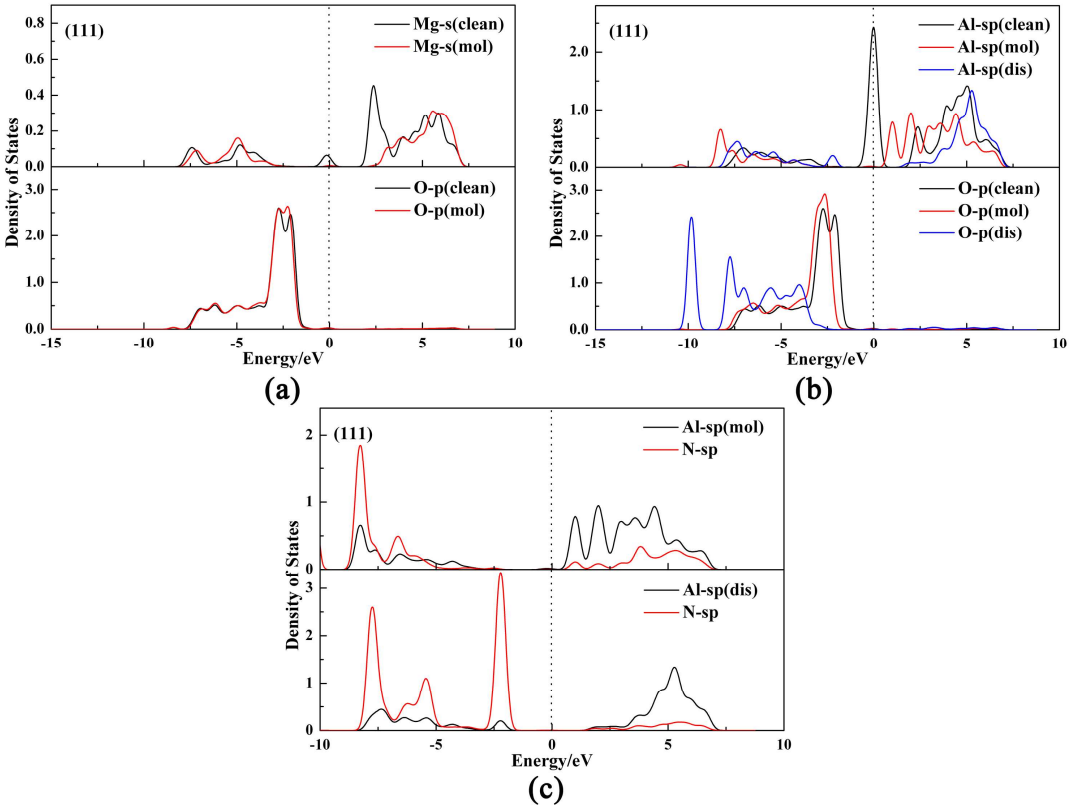

Figure 8. LDOS of (111) surface: **(a)** clean surface and molecular adsorption on Mg_{3c} site, **(b)** clean surface and adsorption on Al_{3c} site, and **(c)** comparison between molecular and dissociated adsorptions on Al_{3c} site.

As seen in Figure 8a and 8b, the surface Al_{3c}-sp state at the Fermi level promoted adsorption, which determined the favorable Al_{3c}-sp active site; there was no obvious surface state on the Mg_{3c} site. As could be observed upon NH_3 dissociation, the downshift of the O_{3c}-sp state indicated that the H-O_{3c} covalent bond formed. For the adsorption on the Al_{3c} site, the H-O_{3c} covalent bond of the dissociation was much stronger than the hydrogen bond of the molecular adsorption. The LDOS in Figure 8c was employed to analyze the different adsorption energies of the molecular and dissociated adsorptions. For the dissociation, it was easy to find a new N-sp state near the Fermi level located at the -2.24-eV position, which came from the left electron state of the dissociated H atom. This was the same as that of the (100) surface. The N-sp state between -8.31 eV and -6.61 eV just shifted slightly to a higher energy between -7.79 eV and -5.47 eV, which was different from the higher up-shift of the N-sp state on the (100) surface. In addition, the intensity of the overlap between the Al_{3c}-sp and N-sp state on the (111) surface (Figure 8c) was larger than the intensity of the overlap between the Mg_{2c}-s and N-sp state on the (100) surface (Figure 4c). In particular, the N-p peak near the Fermi level originated from the orbital splitting of dissociated NH_2 exactly overlapped with the new Al_{3c}-sp peak. Therefore, the adsorption energy of the NH_3 dissociated on the Al_{3c} site was the most thermodynamically favorable.

In order to perform a kinetic investigation of the surface reaction, the transition states for dissociative adsorption were calculated and are listed in Table 6. The activation barriers of the three surfaces were 2.63, 2.93, and 1.88 eV, respectively, with the barrier energy of the (111) surface being the lowest. Therefore, from a dynamic view, the (111) surface was the best surface for ammonia dissociation.

Table 6. Energy barriers for dissociative adsorption on different active sites of perfect and defective surfaces.

(100)	Perfect-Mg_{2c}	Vo_{3c}-Mg_{2c}	Vo_{4c}-Mg_{1c}	-
TS-dis (eV)	2.63	2.82	4.64	-
(110)	Perfect-Al_{4c}	Vo_{3c}-Al_{4c}	-	-
TS-dis (eV)	2.93	2.49	-	-
(111)	Perfect-Al_{3c}	Vo_{3c}-Al_{3c}	Vo_{3c}	Vo_{4c}
TS-dis (eV)	1.88	1.90	1.28	2.22

3.2 NH_3 Adsorption and Dissociation on Defective $MgAl_2O_4$ Surfaces

3.2.1 Structure of Defective $MgAl_2O_4$ Surfaces

This section discusses the NH_3 molecule adsorption on defective $MgAl_2O_4$ surfaces with oxygen vacancies. Five types of oxygen vacancy defects are presented in Figure S8 (ESI): O_{3c} and O_{4c} vacancies on the (100) surface, O_{3c} vacancy on the (110) surface, and O_{3c} and O_{4c} vacancies on the (111) surface. In order to calculate the surface formation energies of an oxygen vacancy, E_{Vo}, we used the following equation:

$$E_{Vo} = -(E_{perf} - E_{def} - \frac{1}{2}E_{O_2})$$

where E_{perf} is the total energy of the perfect clean surface, E_{def} is the total energy of the defective clean surface, and E_{O_2} is the total energy of the free O_2 molecule. Figure 9 presents top views of the oxygen vacancy defect structures and corresponding vacancy formation energies, which are labeled as (100)-Vo_{3c}, (100)-Vo_{4c}, (110)-Vo_{3c}, (111)-Vo_{3c}, and (111)-Vo_{4c}. The (111) surface possessed a lower formation energy than the other two surfaces, which made it easier to form the oxygen vacancy compared to the other two surfaces. The establishment of the oxygen vacancy changed the surface geometry structure, as seen in Figure 9, and the surface symmetry structure was destroyed. In addition, the surface Mulliken charges were also changed after establishing the oxygen vacancy. The value of the charge on the metal site decreased, and the reduction of the charge on the Vo_{4c} surface was higher than that of the Vo_{3c} surface, which would result in the different adsorption energies. However,

the relative values of the Mulliken charges among the three defective surfaces were consistent with those of perfect surfaces. Therefore, the adsorption models for the defective surfaces were similar to the models for perfect surfaces.

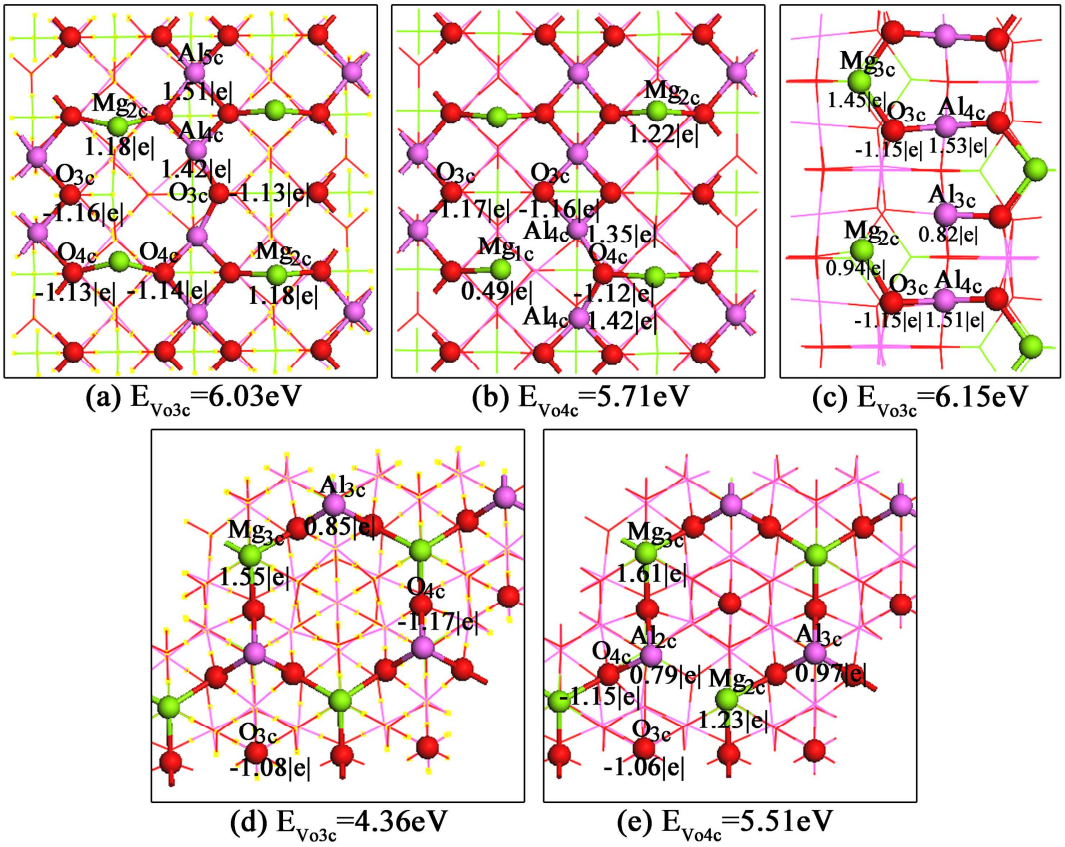

Figure 9. Top views of optimized structures and corresponding surface energies of defective $MgAl_2O_4$ (100) surface **(a, b)**, (110) surface **(c)**, and (111) surface **(d, e)**. The surface vacancy formation energies and Mulliken charges are labeled in the figure.

3.2.2 Interaction of NH_3 with Defective Surfaces

Adsorption on Metal Site: The optimized configurations of the three surfaces are presented in Figures S9-S11 (ESI). It is easy to find the similarity between the defective and perfect surfaces. Surface Mg and Al atoms were still the most important active sites for the adsorption and reaction, and the NH_3 molecule was inclined to be adsorbed on these metal sites. The influence factor for the adsorption did not change: the N-M (metal) bond and H-O covalent band were important forces for adsorption.

The existence of the hydrogen bond would have synergistically promoted the adsorption, whereas the steric hindrance prohibited the adsorption. However, the adsorption energies on the defective surfaces were lower than those on the perfect surfaces. This was because the symmetry of the surface configurations was destroyed, and the charge value of the metal site decreased. With the existence of the oxygen defect, the reduction of the charge value indicated that the electrons partly transferred to the metal site, which changed the surface state on the metal site. As seen in Figure 10, the surface Mg_{2c}-s state decreased on the Vo_{3c} (100) surface, and the surface Mg_{1c}-s state shifted toward a lower energy on the Vo_{4c} (100) surface. The (110) surface Mg_{2c}-s state shifted toward a lower energy on the Vo_{3c} surface. The (111) surface Al_{3c}-sp state changed very little on the Vo_{3c} site, and the Al_{2c}-sp state was split on the Vo_{4c} surface. These findings suggest that the existence of the oxygen vacancy on the surface weakened the effect of the surface state, except for the Vo_{3c} site of the (111) surface. The adsorption energy of the NH_3 dissociated on the Al_{3c} site of the (111) Vo_{3c} surface was 2.27 eV, which was the highest among the defective surfaces.

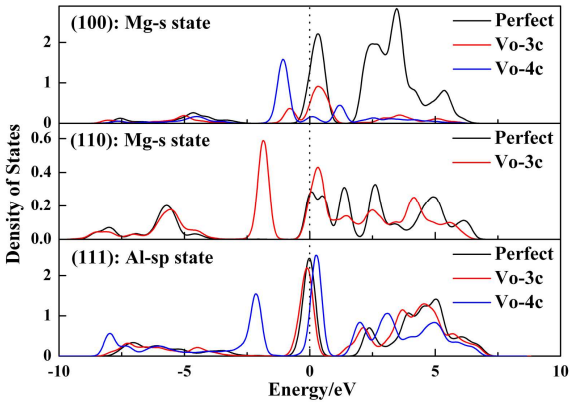

Figure 10. LDOS for active sites on perfect and defective (100), (110), and (111) surfaces without adsorption.

Adsorption on Vacancy Site: In addition to the effect of the metal adsorption site, the oxygen vacancy could also act as an adsorption site. Thus, we further calculated the configurations in relation to the adsorption and dissociation on the Vo_{3c} and Vo_{4c}

sites, as shown in Figure 11. For the (100) and (110) surfaces, a strong steric hindrance could significantly weaken the stability of the adsorption, and the adsorption energies were very low on these two surfaces. This indicated that the vacancy sites for NH_3 adsorption on the (100) and (110) surfaces were not the active sites. The adsorption energies on the defective sites of the (111) surface were relatively higher, because the oxygen vacancy acted as an active site for adsorption and dissociation. For the NH_3 molecular adsorption on the Vo_{3c} site (Figure 11d), the adsorption energy was only 0.61 eV, which suggested that the NH_3 molecule still suffered from some steric hindrance. For the dissociation on the Vo_{3c} site (Figure 11e), the adsorption energy was 2.55 eV. The NH_2 was located at the center with a slight steric hindrance, and the dissociated H combined with the Al_{3c} atom, which resulted in higher adsorption energy. It was impossible for NH_3 molecular adsorption to occur on the Vo_{4c} site because of the strong steric hindrance and competition of the neighboring Al site. For the NH_3 dissociation on the Vo_{4c} site, the adsorption energy was 1.52 eV, which was lower than the dissociation on the Vo_{3c} site. The H-O_{3c} covalent bond played an important role for adsorption, whereas the NH_2 group located between the Al and Mg atoms suffered from resistance because of steric hindrance. A comparison of the adsorptions and reactions for all of these showed that the dissociation on the Vo_{3c} site of the (111) surface was the most favorable adsorption on the oxygen vacancy sites.

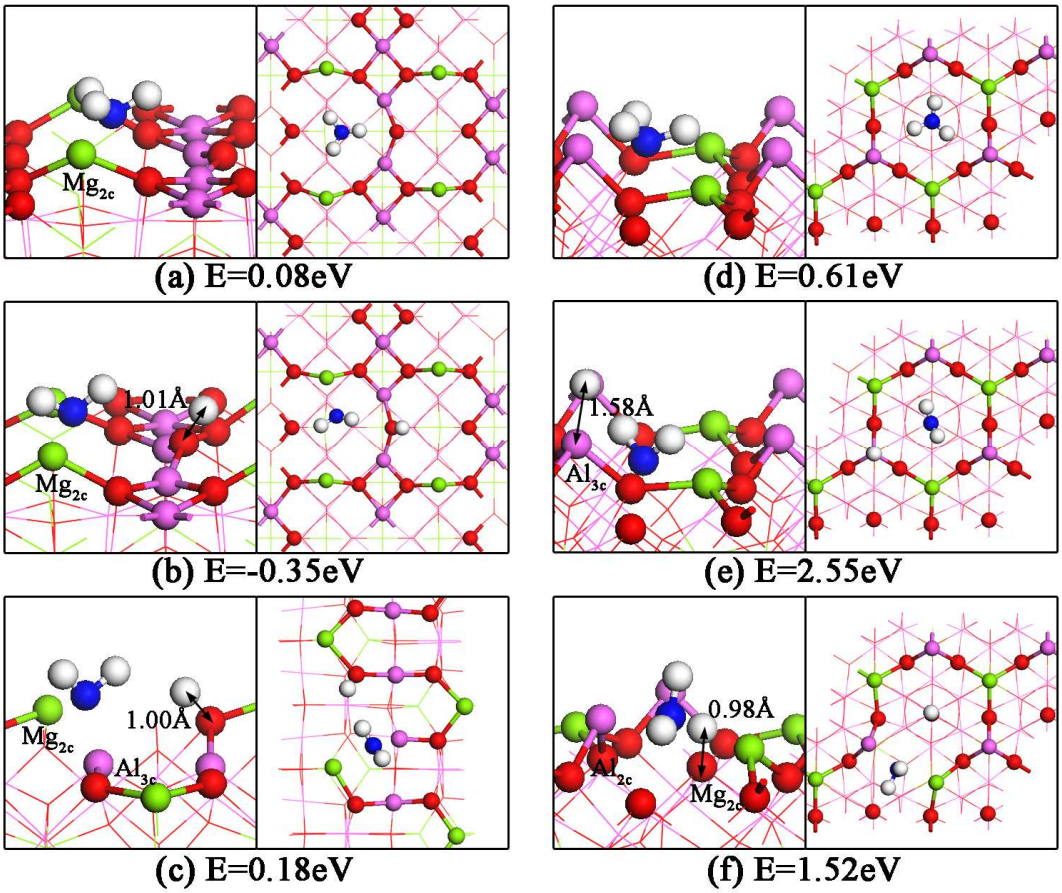

Figure 11. Front and top views of the main adsorption and dissociation configurations and energies of NH_3 on Vo site: **(a)** molecular adsorption on Vo_{3c} site of (100) surface, **(b)** dissociated adsorption on Vo_{3c} site of (100) surface, **(c)** dissociated adsorption on Vo_{3c} site of (110) surface, **(d)** molecular adsorption on Vo_{3c} site of (111) surface, **(e)** dissociated adsorption on Vo_{3c} site of (111) surface, and **(f)** dissociated adsorption on Vo_{4c} site of (111) surface.

After comparing the adsorption energies of the defective surfaces, we came to the conclusion that the adsorption and dissociation on the metal or vacancy sites of the (111) surface were much more favorable than those on the other two surfaces. Table 6 presents the barrier energies of the NH_3 reaction on the Vo_{3c} and Vo_{4c} surfaces. The existence of an oxygen vacancy could lower the potential barrier, especially for the reaction on the (111) surface. The barrier energy on the Vo_{3c} site of the (111) surface was only 1.28 eV, which was much lower than the barrier energy (1.88 eV) on the perfect surface. These results suggested that the establishment of an O_{3c} vacancy on

the (111) surface was dynamically favorable for NH_3 reaction.

4. CONCLUSIONS

To fully understand the mechanism of NH_3 adsorption on $MgAl_2O_4$ surfaces, the density functional theory was employed to investigate the NH_3 adsorption and reaction on perfect and defective (100), (110) and (111) $MgAl_2O_4$ surfaces. The results showed that the adsorption of NH_3 on $MgAl_2O_4$ surfaces was a structure-sensitive reaction. Surface metal atoms acted as the main sites for the adsorption and reaction, while the hydrogen bond had a synergistic effect on the adsorption stability. The surface electronic structure was another important factor for adsorption. The surface state at the Fermi level was an important force for the adsorption, which determined the activated adsorption metal site. In particular, the overlap between the Al_{3c}-sp orbital and N-sp state could significantly promote adsorption on the (111) surface. The coordinated action of the surface geometry and electronic structure stabilized the NH_3 adsorption on the (111) surface. Our work demonstrated that the (111) was the most favorable surface for the NH_3 adsorption and reaction in view of the thermodynamics and dynamics.

The generation of an oxygen vacancy resulted in a reduction in the surface metal charge, which lowered the adsorption stability on the metal site. In addition, the oxygen vacancy acted as an active site for adsorption on the (111) surface. In particular, the NH_3 dissociation on Vo_{3c} site of (111) surface had the lowest reaction barrier. This suggested that the establishment of an oxygen vacancy on the (111) surface was dynamically favorable for the reaction.

In summary, this work suggested that the selection of the exposed surface and oxygen vacancy of $MgAl_2O_4$ was very important for NH_3 adsorption and dissociation. Information about the adsorbate geometries, reaction activities of various surface sites, and specific electronic structure of the surface metal atoms could provide theoretical guidance for the future design of $MgAl_2O_4$ catalysts, as well as for an atomistic-level understanding of other structure-dependent reactions.

ACKNOWLEDGEMENTS

This work was supported by the National Natural Science Foundation of China (Grant No. 21173131), and the Taishan Scholar Project of Shandong Province (China)

REFERENCES

[1] A. K. Avci, D. L. Trimm, Z. I. Onsan, Quantitative Investigation of Catalytic Natural Gas Conversion for Hydrogen Fuel Cell Applications, *Chem. Eng. J.*, 2002, **90**, 77-87.

[2] F. Rosowski, A. Hornung, O. Hinrichsen, D. Herein, M. Muhler, G. Ertl, Ruthenium Ccatalysts for Ammonia Synthesis at High Pressures: Preparation, Characterization, and Power-law Kinetics, *Appl. Catal. A.*, 1997, **151**, 443-460.

[3] J. C. Ganley, F. S. Thomas, E. G. Seebauer, R. I. Masel, A Priori Catalytic Activity Correlations: The Difficult Case of Hydrogen Production from Ammonia, *Catal. Lett.*, 2004, **96**, 117-122.

[4] T. V. Choudhary, C. Sivadinarayana, D. W. Goodman, Catalytic Ammonia Decomposition: CO_x-Free Hydrogen Production for Fuel Cell Applications, *Catal. Lett.*, 2001, **72**, 197-201.

[5] R. Metkemeijer, P. Achard, Comparison of Ammonia and Methanol Applied Indirectly in A Hydrogen Fuel Cell, Int. *J. Hydrogen Energy.*, 1994, **19**, 535-542.

[6] A. Klerke, C. H. Christensen, J. K. Nørskov, T. Vegge, Ammonia for Hydrogen Storage: Challenges and Opportunities, *J. Mater. Chem.*, 2008, **18**, 2304-2310.

[7] L. G. V. Briquet, C. R. A. Catlow, S. A. French, Structure and Reactivity of Aluminum Oxide Supported Nickel Clusters, *J. Phys. Chem. C.*, 2010, **114**, 22155-22158.

[8] J. D. Li, E. Croiset, L. Ricardez-Sandoval, Effect of Metal-Support Interface During CH_4 and H_2 Dissociation on Ni/γ-Al_2O_3: A Density Functional Theory Study, *J. Phys. Chem. C.*, 2013, **117**, 16907-16920.

[9] R. Wischert, P. Laurent, C. Copéret, F. Delbecq, P. Sautet, γ-Alumina: The Essential and Unexpected Role of Water for the Structure, Stability, and Reactivity of "Defect" Sites, *J. Am. Chem. Soc.*, 2012, **134**, 14430-14449.

[10] G. R. Jenness, M. A. Christiansen, S. Caratzoulas, D. G. Vlachos, R. J. Gorte,

Site-Dependent Lewis Acidity of γ-Al_2O_3 and Its Impact on Ethanol Dehydration and Etherification, *J. Phys. Chem. C.*, 2014, **118**, 12899-12907.

[11] D. Cao, Y. Li, J. Wang, H. Jiao, Mechanism of γ-Al_2O_3 Support in CO_2 Reforming of CH_4 A Density Functional Theory Study, *J. Phys. Chem. C.*, 2011, **115**, 225-233.

[12] H. Tan, K. Li, S. Sioud, D. Cha, M. H. Amad, M. N. Hedhili, Z. A. Al-Talla, Synthesis of Ru Nanoparticles Confined in Magnesium Oxide-modified Mesoporous Alumina and Their Enhanced Catalytic Performance during Ammonia Decomposition, *Catal. Commun.*, 2012, **26**, 248-252.

[13] D. Szmigiel, W. Raróg-Pilecka, E. Miskiewicz, Z. Kaszkur, Z. Kowalczyk, Ammonia Decomposition over the Ruthenium Catalysts Deposited on Magnesium-aluminum Spinel, *Appl. Catal. A: Gen.*, 2004, **264**, 59-63.

[14] J. M. H. Lo, T. Ziegler, P. D. Clark, SO_2 Adsorption and Transformations on γ-Al_2O_3 Surfaces: A Density Functional Theory Study, *J. Phys. Chem. C.*, 2010, **114**, 10444-10454.

[15] J. Handzlik, P. Sautet, Structure of Dimeric Molybdenum (VI) Oxide Species on γ-Alumina: A Periodic Density Functional Theory Study, *J. Phys. Chem. C.*, 2010, **114**, 19406-19414.

[16] D. H. Mei, V. A. Glezakou, V. Lebarbier, L. Kovarik, H. Y. Wan, K. O. Albrecht, M. Gerber, R. Rousseau, R. A. Dagle, Highly Active and Stable $MgAl_2O_4$-supported Rh and Ir Catalysts for Methane Steam Reforming: A Combined Experimental and Theoretical Study, *J. Catal.*, 2014, **316**, 11-23.

[17] F. Frechard, R. A. van Santen, A. Siokou; J. W. Niemantsverdriet, J. Hafner, Adsorption of Ammonia on the Rhodium (111), (100), and Stepped (100) Surfaces: An Ab Initio and Experimental Study, *J. Chem. Phys.*, 1999, **111**, 8124-8130.

[18] S. B. Tang, Z. X. Cao, Adsorption and Dissociation of Ammonia on Graphene Oxides: A First-principle Study, *J. Phys. Chem. C.*, 2012, **16**, 8778-8791.

[19] S. Wendt, R. Schaub, J. Matthiesen, E. K. Vestergaard, E. Wahlstrom, M. D. Rasmussen, P. Thostrup, L. M. Molina, E. Laegsgaard, I. Stensgaard, B. Hammer, F. Besenbacher, Oxygen vacancies on TiO_2 (110) and their interaction with H2O and O2:

A combined high-resolution STM and DFT study, *Surf. Sci.* 2005, **598**, 226-245.

[20] C. T. Campbell, C. H. F. Peden, Oxygen vacancies and catalysis on ceria surfaces, *Science*, 2005, **309**, 713-714.

[21] M. Fronzi, S. Piccinin, B. Delley, E. Traversa, C. Stampfl, Water adsorption on the stoichiometric and reduced CeO_2 (111) surface: a first-principles investigation, *Phys. Chem. Chem. Phys.* 2009, **11**, 9188-9199.

[22] C. H. Sun, T. Liao, G. Q. Lu, S. C. Smith, The Role of Atomic Vacancy on Water Dissociation over Titanium Dioxide Nanosheet: A Density Functional Theory Study, *J. Phys. Chem. C*, 2012, **116**, 2477-2482.

[23] R. Schaub, P. Thostrup, N. Lopez, E. Laegsgaard, I. Stensgaard, J. K. Norskov, F. Besenbacher, Oxygen Vacancies as Active Sites for Water Dissociation on Rutile TiO_2 (110), *Phys. Rev. Lett.*, 2001, **87**, 266104-1-4.

[24] M. C. Payne, M. P. Teter, D. C. Allan, T. A. Arias, J. D. Joannopoulos, Iterative Minimization Techniques for Ab Initio Total-energy Calculations: Molecular Dynamics and Conjugate Gradients, *Rev. Mod. Phys.*, 1992, **64**, 1045-1097.

[25] M. Segall, P. Lindan, M. Probert, M. Pickard, C. Pickard, P. Hasnip, S. Clark, M. Payne, First-principles Simulation: Ideas, Illustrations and the CASTEP Code, *J. Phys.: Condens. Matter.*, 2002, **14**, 2717-2743.

[26] S. J. Clark, M. D. Segall, C. J. Pickard, P. J. Hasnip, M. J. Probert, K. Refson, M. C. Payne, First Principles Methods Using CASTEP, Z. *Kristallogr.*, 2005, **220**, 567-570.

[27] J. P. Perdew, J. A. Chevary, S. H. Vosko, A. K. Jackson, R. M. Pederson, D. J. Singh, C. Fiolhais, Atoms, Molecules, Solids, and Surfaces: Applications of the Generalized Gradient Approximation for Exchange and Correlation, *Phys. Rev. B.*, 1992, **46**, 6671-6687.

[28] J. P. Perdew, Y. Wang, Accurate and Simple Analytic Representation of the Electron-gas Correlation Energy, *Phys. Rev. B.,* 1992, **45**, 13244-13249.

[29] H. J. Monkhorst, J. D. Pack, Special Points for Brillouin-zone Integrations, *Phys. Rev. B.*, 1976, **13**, 5188-5192.

[30] T. Yamanaka, Y. Takéuchi, M. Tokonami, Anharmonic Thermal Vibrations of

Atoms in $MgAl_2O_4$ Spinel at Temperatures up to 1933 K, *Acta Cryst.*, 1984, **B40**, 96-102.

[31] C. G. Zhou, J. Y. Li, S. Chen, J. P. Wu, K. R. Heier, H. S. Cheng, First-Principles Study on Water and Oxygen Adsorption on Surfaces of Indium Oxide and Indium Tin Oxide Nanoparticles, *J. Phys. Chem. C.*, 2008, **112**, 14015-14020.

[32] P. Li, X. Zhao, C. J. Jia, H. G. Sun, L. M. Sun, X. F. Cheng, L. Liu and W. L. Fan, $ZnWO_4$/BiOI heterostructures with highly efficient visible light photocatalytic activity: the case of interface lattice and energy level match, *J. Mater. Chem. A*, 2013,**1**, 3421-3429.

[33] M. K. Rasmussen, A. S. Foster, B. Hinnemann, F. F. Canova, S. Helveg, K. Meinander, N. M. Martin, J. Knudsen, A. Vlad, E. Lundgren, A. Stierle, F. Besenbacher and J. V. Lauritsen, Stable Cation Inversion at the $MgAl_2O_4$ (100) Surface, *Phys. Rev. Lett.*, 2011, **107**, 036102-1-4.

[34] Q. L. Tang and Q. H. Luo, Adsorption of CO_2 at ZnO: A Surface Structure Effect from DFT+U Calculations, *J. Phys. Chem. C*, 2013, **117**, 22954-22966.

[35] M. M. Rodriguez, X. H. Peng, L. J. Liu, Y. Li and J. M. Andino, A Density Functional Theory and Experimental Study of CO_2 Interaction with Brookite TiO_2, *J. Phys. Chem. C*, 2012, **116**, 19755-19764.

[36] D. Sanchez-Portal, E. Artacho, J. M. Soler, Projection of Plane-wave Calculations into Atomic Orbitals, *Solid State Commun.*, 1995, **95,** 685-690.

[37] X. Gonze, First-principles Responses of Solids to Atomic Displacement and Homogeneous Electric Fields: Implementation of A Conjugate-gradient Algorithm, *Phys. Rev. B.*, 1997, **55**, 10337-10354.

[38] T. A. Halgren, W. N. Lipscomb, The Synchronous-transit Method for Determining Reaction Pathways and Locating Molecular Transition States, *Chem. Phys. Lett.*, 1977, **49**, 225-232.

[39]. V. P. Indrakanti, J. D. Kubicki, H. H. Schobert, Photoinduced activation of CO_2 on Ti-based heterogeneous catalysts: Current state, chemical physics-based insights and outlook, *Energy Environ. Sci.*, 2009, **2**, 745-758.

[40] K. Hadidi, R. Hancke, T. Norby, A. E. Gunnces, O. M. Lovvik, Atomistic Study

of $LaNbO_4$; Surface Properties and Hydrogen Adsorption, *Int. J. Hydrogen Energy*, 2012, **37**, 6674-6685.